Cure Kinetics of a High Epoxide/Hydroxyl Group-Ratio Bisphenol A Epoxy Resin–Anhydride System by Infrared Absorption Spectroscopy

GARY C. STEVENS, *Central Electricity Research Laboratories, Leatherhead, Surrey, KT22 7SE, United Kingdom.*

Synopsis

An infrared absorption spectroscopy study of the curing (gelation and postcure) kinetics of a high (4.7) epoxide/hydroxyl group-ratio diglycidyl ether of bisphenol A (DGEBA)–mixed anhydride epoxy resin system is reported. Peak assignments to molecular vibrational modes are given for the range 400–4000 cm^{-1}, and the optical density behavior of all peaks during reaction is discussed in detail. Chemical reaction was found to follow consecutive-step addition esterification and simultaneous addition etherification. Epoxide hydroxyl-group and carboxylic acid-dimer hydrogen bonding was found to occur. The gelation phase of reaction is complex, exhibiting rapid initial hydroxyl–anhydride reactions followed by S-shaped kinetics approaching an incompletely reacted limit. Postcure exhibits functional group kinetic behavior similar to that occurring in low epoxide/hydroxyl group-ratio bisphenol A epoxy resin–phthalic anhydride systems and produces similar final chemical structures. The reaction behavior of low and high epoxide/hydroxyl group-ratio bisphenol A epoxy resin–anhydride systems arises from an hydroxyl group-limited inhomogeneous reaction mechanism involving bisphenol A epoxy resin molecular aggregates. The importance of free hydroxyl group content is discussed.

INTRODUCTION

The preceding report (herein referred to as part I) considered the reaction of a low epoxide/hydroxyl group-ratio bisphenol A epoxy resin–phthalic anhydride epoxy resin system as studied by infrared spectroscopy. The observations were consistent with the basic chemical scheme proposed by Fisch and Hofmann[1] and supported a previously proposed free hydroxyl group-limited colloidal-type reaction mechanism.[2] This article deals with a chemically related but high epoxide/hydroxyl (E/H)-group ratio bisphenol A resin–anhydride system in which

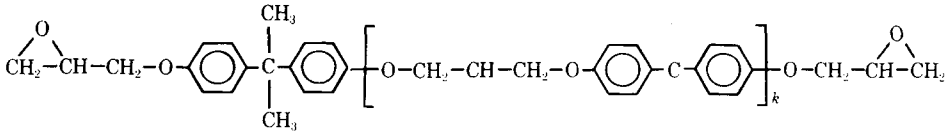

Journal of Applied Polymer Science, Vol. 26, 4279–4297 (1981)
 CCC 0021-8995/81/124279-19$01.90

the $k = 0$ oligomer fraction dominates the molecular weight distribution. In contrast to the low E/H ratio resin system considered in part I, this system displays weaker free hydroxyl-group hydrogen bonding. Variable-temperature and dissolution light scattering studies indicate the presence of small (<20 nm) molecular aggregates in the unreacted resin system, consistent with stronger hydrogen bonding and larger aggregates in the low E/H ratio system.[3]

The epoxy resin under consideration is the Ciba–Geigy CY207–HT903 system. The CY207 resin component contains an epoxide content of 4.4 to 4.6 mol/kg, a free hydroxyl content of 0.7 to 1.2 mol/kg, and a $k = 0$ mass fraction of about 61%. HT903 is an anhydride mixture containing phthalic anhydride (PA) and a larger proportion of tetrahydrophthalic anhydride (THPA):

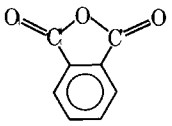

PA

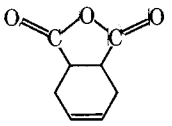

THPA

Hydrolysis of THPA to 4-cyclohexene-1,2-dicarboxylic acid (CDA) accounts for the PA range observed.

PA and THPA will compete for reaction with the resin free hydroxyl groups according to the Fisch and Hofmann or Tanaka and Kakiuchi schemes described in part I. The former scheme applies to the low E/H DGEBA–PA system discussed in part I, and the anhydride competition may be expressed by the following equations:

$$A + B_1 \xrightarrow{k_1} C_1 \tag{1}$$

$$A + B_2 \xrightarrow{k_1'} C_2 \tag{2}$$

$$C_1 + D \xrightarrow{k_2} E_1(A) \tag{3}$$

$$C_2 + D \xrightarrow{k_2'} E_2(A) \tag{4}$$

for addition esterification and

$$A + D \xrightarrow[B_1, B_2, C_1, C_2]{k_3} F(A) \tag{5}$$

for addition etherification, where A, D, and F are, respectively, hydroxyl group, epoxide group, and ether linkages; and B_1, B_2, C_1, C_2 and E_1, E_2 are the respective PA and THPA anhydride components, their corresponding monoester groups (containing carboxylic acid groups), and diester linkages. Flory's general assumption of equal reactivity of similar functional groups cannot be applied to the two anhydrides. If different anhydride and carboxylic acid reactivities are anticipated, then $k_1 \neq k_1'$ and $k_2 \neq k_2'$, and subsequent secondary hydroxyl groups (A) may also exhibit different reactivity. Complex kinetic behavior is expected unless rate control is exercised by one reaction or component. Anhy-

dride and hydroxyl group behavior are particularly important in distinguishing reaction mechanisms. In the low E/H ratio system reported in part I, [A] ~ [B] ~ [D], which in the absence of group limitation imposes second-order kinetics during the initial phase of anhydride consumption. Hydroxyl group limitation or colloid-type X + Y → Y reactions would impose first-order kinetic behavior. In the CY207–HT903 case considered here, [A] ≪ [B] ~ [D]; and in the absence of PA–THPA competition, first-order kinetic behavior would be expected in the absence of an inhomogeneous reaction mechanism.

The CY207–HT903 system also differs from that in part I in that the recommended and commonly adopted cure cycle involves a so called "gelation" phase followed by a higher temperature "postcure" phase. The commonly used reaction conditions were applied here.

EXPERIMENTAL

The chemical characterization of the CY207 bisphenol A epoxy resin is described in part I. Differential scanning calorimetry, infrared spectroscopy, and chemical analysis identified HT903 as a low melting-point PA–THPA mixture containing variable but small quantities of higher melting-point CDA. CY207 and HT903 were repeatedly pressure filtered through 0.2 μm PTFE filters in dry nitrogen. The former was filtered at 400 K and subsequently exhaustively stirred and evacuated at the same temperature to degas and remove volatile impurities. HT903 was filtered at 363 K and then recrystallized and refiltered several times, which proved effective in removing CDA impurities. The CY207–HT903 reactant mass ratio was that recommended by Ciba–Geigy, 100:60 pbw. This corresponds to an epoxide:anhydride molar reaction stoichiometry of 1:0.91. The components were mixed in the liquid phase at 5 K above the gelation temperature and rigorously stirred and partially evacuated. Gelation and postcure temperatures of 353 and 393 K, respectively, were used and short and long gelation times considered. Reaction samples and infrared sample preparation and spectral referencing were as described in part I.

Chemical group optical density comparisons between the CT200–HT901 system of part I and the CY207–HT903 system was undertaken requiring intersystem optical density referencing. An optical-density normalization factor was obtained by using the molecular weight distribution information summarized in part I and the resin:hardener mass ratios. This assumes that the extinction coefficients of the infrared referencing peaks are independent of oligomer size and solvent reactions. Referencing was achieved through the resin methyl peaks at 2962 and 1382 cm^{-1} and the phenyl group peaks at 1605, 1580, and 830 cm^{-1}.

INFRARED PEAK ASSIGNMENTS AND OPTICAL DENSITIES

The infrared spectra of the CY207 andHT903 components were obtained separately. The resin and phthalic anhydride peak assignments were discussed in part I. No complete assignment of the infrared vibrational modes of THPA has been reported so these peaks were identified by default. During reaction a number of new peaks appeared and were assigned by consideration of the likely reaction products summarized in part I and the literature sources contained

therein. Figure 1 illustrates the nature of the spectral changes observed during gelation and postcure and Table I contains the respective peak assignments and their corresponding optical density or range during gelation and postcure and referenced with respect to CT200–HT901. In this case the gelation period optical density range is for a 48-h period, but the postcure range is quoted for a standard 18-h gelation period.

In contrast to the CT200 resin, CY207 contains a dominating $k = 0$ resin fraction producing a larger epoxide group content, allowing this groups kinetics to be followed during reaction. Also, the gelation period and initial postcure exhibit slow overall reaction rates allowing free hydroxyl-group behavior to be followed in greater detail prior to physical gelation of the system. Another interesting difference is that PA and THPA compete for available free hydroxyl groups. Both are distinguishable spectrally, and this competition may be followed. However, their respective carboxylic groups and monoester linkages could not be differentiated.

As in the CT200–HT901 system, on additon of HT903 and CY207, associated (hydrogen-bonded) carboxylic acid-group spectral contributions occurred centered at 3000 and 2550 cm^{-1}. However, in this case the $\nu_{C=O}$ peak at 1705 cm^{-1} was sufficiently strong to use. This latter peak provides a total carboyxlic acid group monitor distinct from the associated acid contributions. The 3500 cm^{-1} ν_{O-H} free hydroxyl-peak optical density for several nonreacted CY207 spectra referenced to the reaction values using the 2962, 1605, 1508, 1038, and 830 cm^{-1} peaks allowed a prereaction estimate of 0.028 for its optical density, compared with the constant initial value of 0.024 during gelation.

Aside from the THPA component, the peak assignment discussion found in the preceding report is applicable to the CY207–HT903 system, and Table I may be used directly without further discussion.

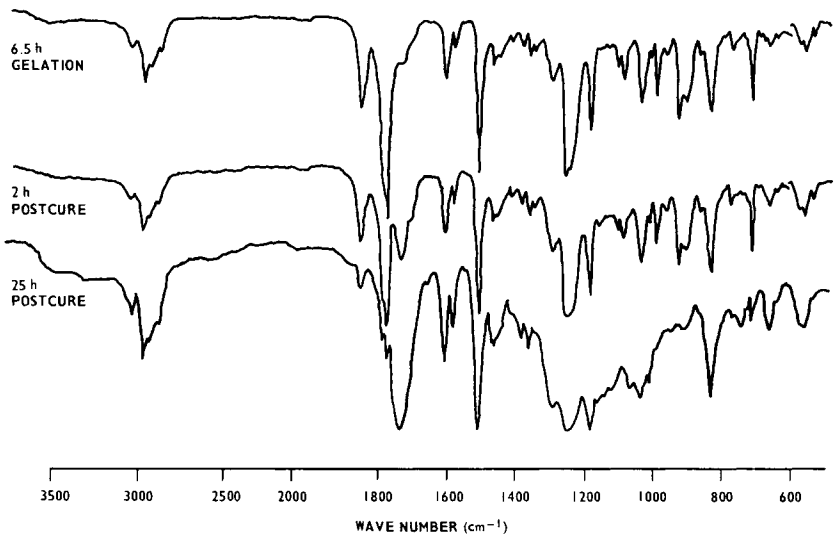

Fig. 1. Infrared absorption spectra of CY207–HT903 during gelation and subsequent postcure; spectra recorded at room temperature.

TABLE I
CY207–HT903 Infrared Spectral Peak Assignments and Optical Density Behavior During Gelation (up to 48 h) and Postcure (After 18 h Gelation)

Peak, cm^{-1}	Assignment	Optical Density Range	
		Celation	Postcure
3500	ν_{O-H}	0.028 ↓ Step 0.024 → 0.014	0.0215 → ?
3000	Associated acid ν_{O-H}	0 → 0.045	0.025 → 0.043 → 0.03
2550	Associated acid ν_{C-O}, δ_{O-H} combination	0 → 0.0125	0.008 → 0.017 → 0.009
2962	ν_{C-H} methyl assymetric stretch	0.1	
1850	anhydride $\nu_{C=O}$	0.2 → 0.134	0.17 → 0
1772	Anhydride $\nu_{C=O}$	0.7 → 0.48	0.55 → 0
1732	Aromatic/total ester $\nu_{C=O}$	0 → 0.23	18 h gelation: 0.15 → 0.35 48 h gelation: 0.23 → 0.45
1705 (undeconvoluted)	Carboxylic acid $\nu_{C=O}$	0 → 0.14	0.08 → (0.175) → (0.125)
1605	Aromatic $\nu_{C=C}$	0.121	
1578	Aromatic $\nu_{C=C}$	0.06	
1508	Aromatic $\nu_{C=C}$	0.26	
1460	Aromatic $\nu_{C=C}$	0.073	
1468	P.A. ν_{C-C}	—	0.046 → 0.029
1410	Epoxide —CH_2 γ_{CH}	—	0.023 → 0
1345	δ_{C-H}	0.033 → 0.018	0.023 → 0
1382	—CH_3 Symm. def.	0.027	
1360	Ether methylene δ_{C-H}	0.047	
1295	δ_{-OH}, γ_{CH_2}	0.075	
1257	Anhydride ν_{C-O-C} Epoxide ν_{C-O-C}	—	
1245	Aromatic ether ν_{C-O} (aryl)	0.26	
1182	Aromatic (resin) δ_{C-H} in-plane	0.129	
1104	Aromatic (PA) δ_{C-H}	0.047 → 0.015	0.034 → 0
1088	THPA δ_{C-H}	0.069 → 0.037	0.056 → 0
1032	Aromatic δ_{C-H} Aromatic ether ν_{C-O} (alkyl)	0.108	
1010	Aromatic δ_{C-H}	—	
1160	Saturated ether ν_{C-O-C}	0.054 → 0.11	0.055 → 0.3
1140	ν_{C-O-C}	0.048 → 0.09	0.05 → 0.3
1120	Branched ether	0.048 → 0.088	0.05 → 0.3
1065	Branched ether	—	0.06 → 0.23
998	THPA	0.1 → 0.065	0.09 → 0
962	THPA	0.0365 → 0.015	0.026 → 0
928	THPA	—	0.155 → 0
900	PA ν_{C-O}	0.125	0.122 → 0

TABLE I
(*Continued from previous page.*)

Peak, cm^{-1}	Assignment	Optical Density Range	
		Celation	Postcure
862	Epoxide	0.046 → 0.29	0.035 → 0
830	Aromatic (resin) δ_{C-H} (out-of-plane)	0.169	
945	Carboxylic δ_{O-H}	—	0.02 → 0.11
990	Ester γ-skeletal	—	0.03 → 0.15
770	THPA	0.048 → 0.03	0.035 → 0.022
728	THPA γ_{C-H}	0.048 → 0.025	0.03 → 0
712	PA γ_{C-H}	0.16 → 0.129	0.132 → 0.018
740	—	—	0.01 → 0.05
688	—	0.022 → 0.009	0.007 → 0
660	—	0.043	
535	PA δ_{CCC}	0.05 → 0.02	0.038 → 0

OPTICAL DENSITY KINETICS OF CURE

Use is made of the reaction kinetic and extent of reaction equations and definitions given in part I. Spectral normalization included the use of the following resin peaks: 2962, 1605, 1578, 1460, 1382, and 830 cm^{-1}.

Hydroxyl and Carboxylic Acid Group Behavior

Infrared spectral observations after mixing indicated the presence of hydrogen-bonded carboxylic acid species and aromatic ester groups. In this case, the 3000 and 2550 cm^{-1} associated carboxylic peaks were accompanied by a resolvable 1705 cm^{-1} peak which was just discernable in the CT200 system. This suggests that the latter peak results from all carboxylic groups and the former peaks from associated species principally. The 80°C gelation behavior of these three peaks is illustrated in Figure 2, and the subsequent 18-h gelation, 120°C postcure behavior is illustrated in the summary diagram of Figure 10. In gelation, the steplike appearance of the groups is obvious, and the 2250 and 3000 cm^{-1} peaks indicate a possible plateau region during the first 6 h of reaction which is not apparent in the 1705 cm^{-1} peak behavior. During gelation, the carboxylic acid group concentration increases slowly, approaching a limit at long times. During postcure, similar increase and peaked behavior are observed, although the 2550 cm^{-1} peak displays more peaked behavior while the 1705 cm^{-1} peak produces more shallow response. However, deconvolution of the 1705 cm^{-1} peak is required to assert detailed behavior. It is interesting that the 2550 and 3000 cm^{-1} optical densities during postcure start and finish at the same value.

On mixing, an immediate change in the free hydroxyl-group optical density is also found. Consideration of before-cure data and the initial gelation-period free hydroxyl ν_{O-H} data shown in Figure 3 indicates a step change from 0.028 to 0.024, a change of about 14%. The 0.028 value agrees with that expected from

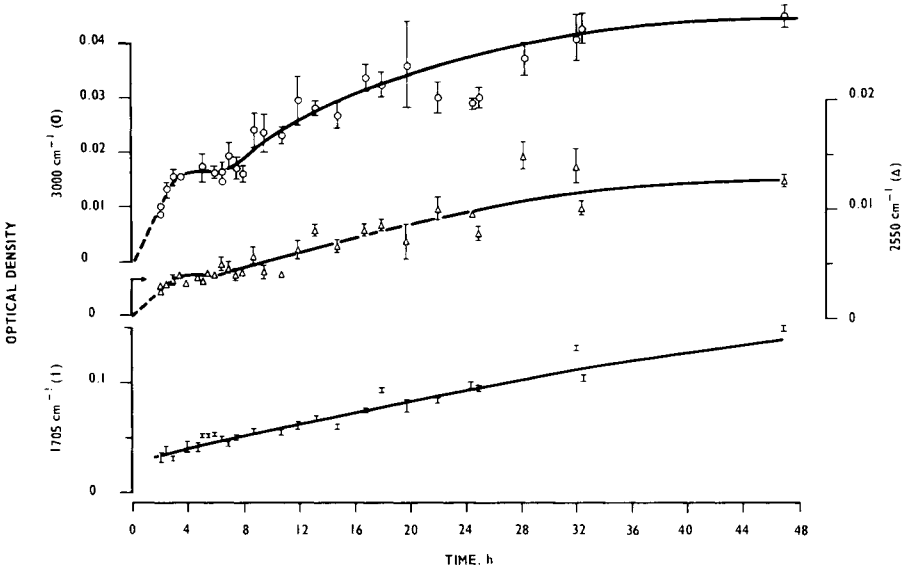

Fig. 2. Carboxylic acid peak optical density behavior during gelation at 80°C.

the CY207 system in comparison with the CT200 and corresponds to a free hydroxyl content of about 1.1 mol/kg, confirming the presence of hydroxyl-containing DGEBA endgroup impurities. The subsequent gelation period exhibits an induction period followed by a decline. On transferring to postcure after 18 h of gelation, a further hydroxyl-group rapid consumption occurs accounting for about 36% of the groups available. The hydroxyl group content then increases after 4 h, approaching its starting value. Unfortunately, physical gelation occurred after 7.5 h of postcure, necessitating powder sample preparation making further hydroxyl group determination unfavorable.

Epoxide Groups

During gelation, the 862 and 1345 cm^{-1} peaks produce the induction period behavior summarized in Figure 9. The corresponding postcure behavior typified by the 1345 and 1410 cm^{-1} peaks is also shown (in Fig. 10) to display S-shaped kinetics where the starting value corresponds to the 18-h gelation point, implying no step change in passing from gelation to postcure. The 1345 and 1410 cm^{-1} peaks exhibited the same reaction extent behavior to which no simple kinetics applied.

Anhydride Groups

In this case, information can be gained on the behavior of the total anhydride content using the 1772 and 1850 cm^{-1} peaks and the individual THPA and PA components. However, only a small number of the available peaks are reliable due to peak overlap. Thus, the 1850 cm^{-1} peak was used for the total anhydride behavior, the 712 and 900 cm^{-1} peaks were used for PA, and the 927 and 988 cm^{-1} peaks were used for THPA. The gelation behavior of the three species is illus-

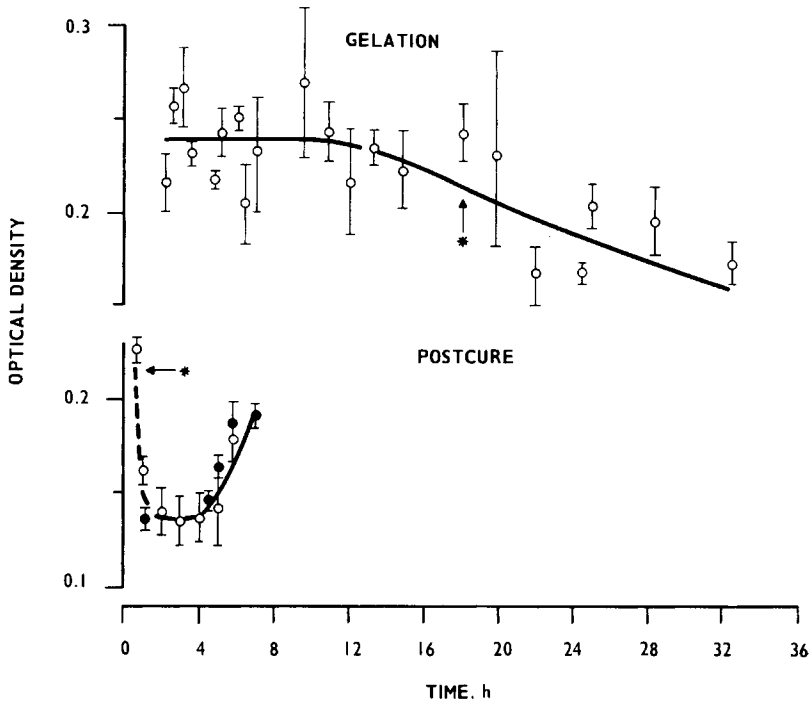

Fig. 3. Free hydroxyl ν_{O-H} optical density behavior during gelation at 80°C and postcure at 120°C after 18 h gelation.

trated in Figure 4. The postcure reaction extent and kinetic plots for PA and THPA total anhydride are also shown in Figures 5 and 6, respectively.

During gelation, PA and THPA display an induction period the extent of which is difficult to assess due to data inaccuracy. Extended gelation shows that a limiting anhydride consumption is reached. At this point, about 22% of the PA and 35% of the THPA initially present have reacted. This is proportionate to their initial mass ratios and should account for about 30% total anhydride; the 1850 and 1772 cm^{-1} peaks indicate 31 and 33%, respectively. This indicates similar overall reactivity of the two anhydrides. However, in gelation the induction period of PA is shortest, whereas during postcure PA displays a slight induction region whereas THPA does not, although both components display half-order consumption kinetics during postcure and exhibit the same slope. Clearly, more detailed behavior occurs. The PA does not fully react, and about 12% remains at the end of cure, accounting for about 4.8% of the total anhydride content, in reasonable agreement with the 3.2% indicated by the 1850 cm^{-1} peak. Total anhydride consumption follows first-order kinetics in the postcure reaction extent range 0.24 to 0.83, with a rate constant of 2.9×10^{-5} s^{-1}.

Ester

In contrast to the CT200–HT901 system, the diester γ-skeletal peak at 990 cm^{-1} parallels the total ester behavior during postcure. However, it is noted that the 988 cm^{-1} THPA peak overlaps, but this is not considered serious because

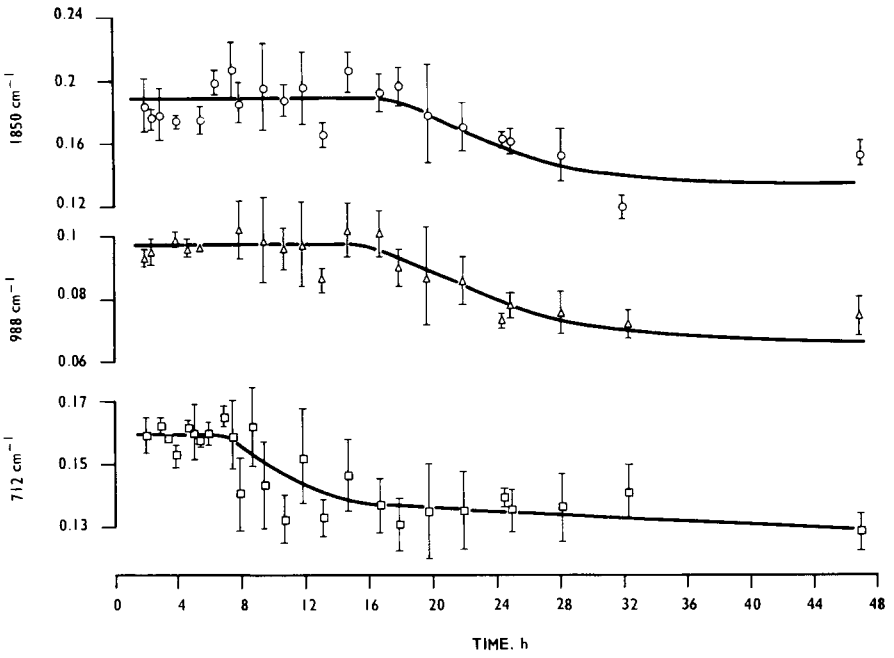

Fig. 4. Total anhydride, THPA, and PA optical density behavior during gelation at 80°C.

the latter is discernible as a peak whereas the 990 cm^{-1} peak is a broad band discernible as a baseline increase.

The total ester $\nu_{C=O}$ 1732 cm^{-1} peak optical density variation during gelation and postcure is summarized in Figures 9 and 10. At the start of gelation, the step behavior agrees with the rapid hydroxyl consumption. Subsequently, it approaches a limiting value at long gelation times, agreeing with the anhydride behavior. Postcure displays the reaction extent and kinetic plots illustrated in Figure 7. First-order behavior extends over the complete reaction with a rate constant of 4×10^{-5} s^{-1}. In this case, the longer gelation period of 48 h leads to a larger final ester content as shown in Table II: the reaction kinetics are similar to those of the shorter gelation period.

Branched Ether

The branched ether peaks at 1120 and 1140 cm^{-1} exhibit the gelation and postcure behavior summarized in Figures 9 and 10. In addition to these peaks another at 1160 cm^{-1} appears and parallels the two above. This was assigned to a saturated ether ν_{C-O-C} mode. A very long induction period is present followed by a simple step reaction to a constant value at long gelation times. During postcure, the simple sigmoid behavior produces the reaction extent and kinetic plots of Figure 8. Overall, half-order reaction kinetics apply, but initially a first-order rate constant may be described, as in the CT200–HT901 system, which is about 1.1×10^{-5} s^{-1}.

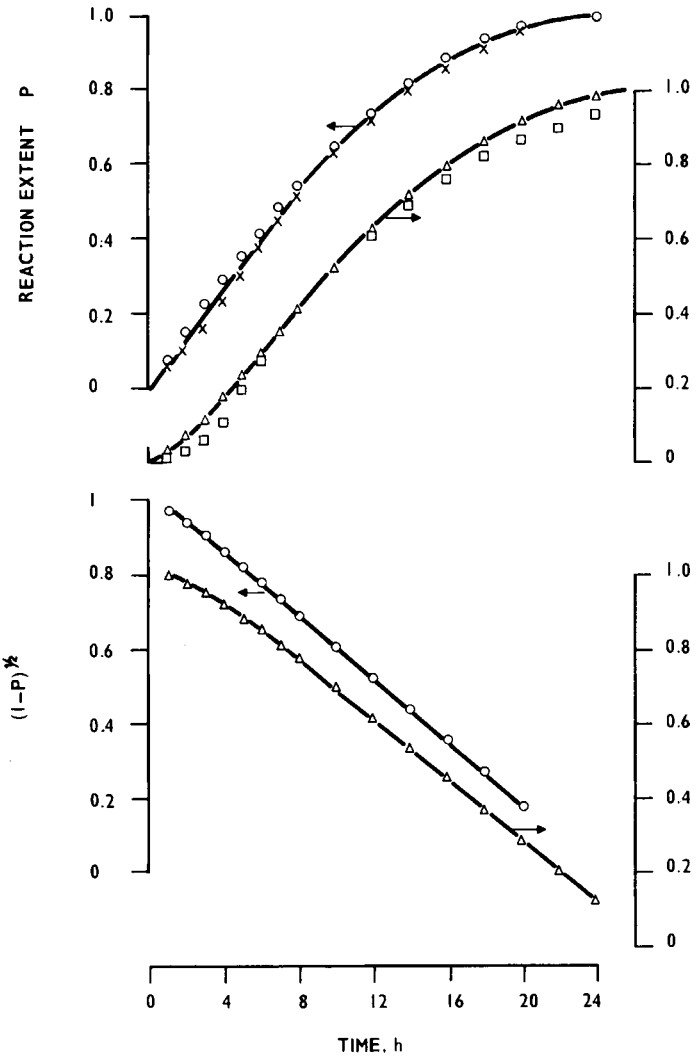

Fig. 5. THPA and PA postcure reaction extent and half-order kinetic plots: THPA: (○) 988 cm^{-1}; (×) PA: (△) 900 cm^{-1}; (+) 712 cm^{-1}.

DISCUSSION

It is useful to discuss the gelation and postcure regions separately and finally compare the reaction behavior and final chemical structure of the CT200-HT901 and CY207-HT903 systems.

Gelation Period

The chemical group optical density behavior during gelation is summarized in Figure 9, where the total carboxylic acid group behavior overlays the total ester behavior and is distinguished from the hydrogen-bonded COOH behavior. The rapid initial carboxylic group formation is accompanied by rapid hydroxyl group consumption involving about 14% of the hydroxyl groups available and also by

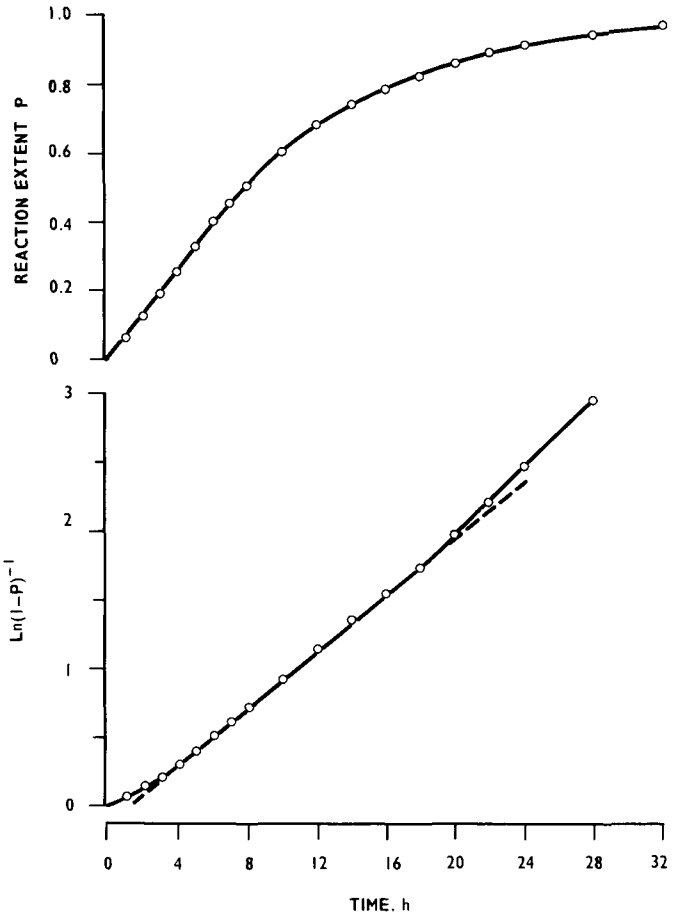

Fig. 6. Total anhydride postcure reaction extent and first-order kinetic plot.

the rapid appearance of aromatic ester groups consistent with an initial rapid monoester addition reaction. After this rapid reaction, the epoxide and anhydride group contents remain constant and the associated carboxylic acid groups and hydroxyl group contents appear constant also. However, data inaccuracy in all cases limits definitive discussion about these induction periods. Nevertheless, the behavior indicates that immediate reaction creates a carboxylic acid reservoir and that a temporary chemical equilibrium exists. Continuation may require the diester reaction to proceed and regenerate additional free hydroxyl groups to retrigger reaction progression by further anhydride reaction. However, the diester contributions at 990 cm^{-1} do not become apparent until postcure, and the total ester behavior parallels the total carboxylic acid behavior during gelation, suggesting some other mechanism. The reaction restarts after about 6 h, which corresponds to the minimum observed in the light scattering dissymmetry of the material which occurred after dramatic changes on harder addition in both CT200 and CY207.[4] This suggests that a matrix effect retriggers

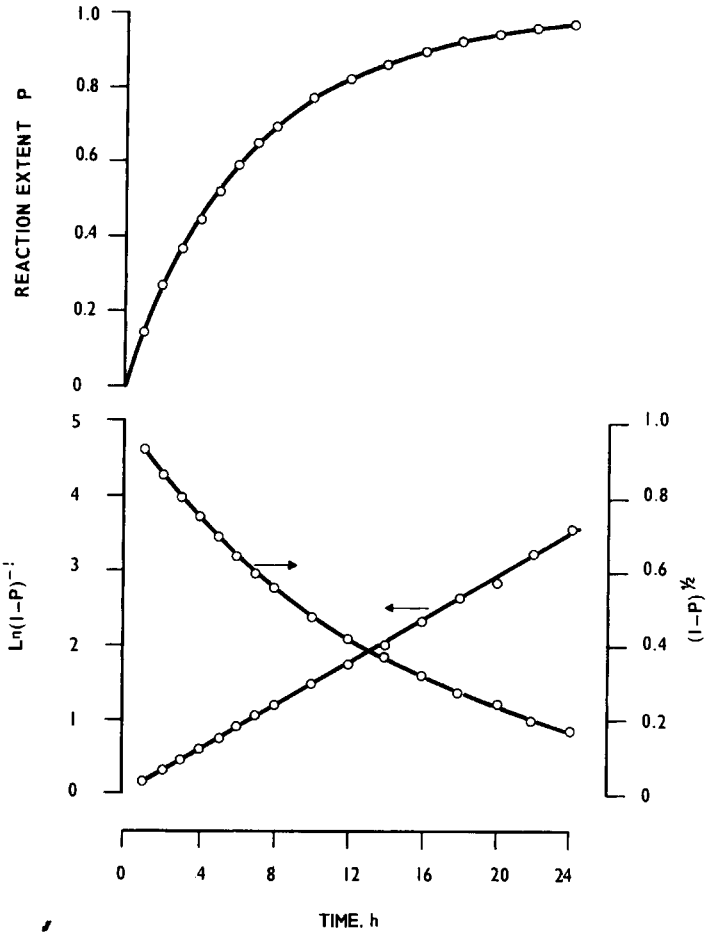

Fig. 7. Ester postcure reaction extent and first- and half-order kinetic plots.

the reaction. This will be discussed further in following reports dealing with the light scattering behavior.

As reaction proceeds, anhydride, epoxide, and hydroxyl consumptions occur such that at the end of gelation, when the reaction rate is very slow, PA and THPA have reacted by amounts proportionate to their starting concentrations. The esterification reaction exhibits an extended induction period followed by a step increase to a constant level in line with anhydride, epoxide and carboxylic group leveling. This approach of the overall reaction to a new chemical equilibrium occurs with the material still in the liquid phase, i.e., no actual gelation has occurred. The system is potentially reactive, and the existence of a matrix-controlled limitation or matrix phase separation (e.g., gel–sol separation with the loss of solution properties) mechanism appears appropriate. Both mechanisms involve an unreactive interface between reacted and unreacted fractions, and this will be discussed further below.

TABLE II
Comparison of Cure Behavior and Final Chemical Structures of CT200–HT901 and CY207–HT903 (After 18 h Gelation)

	Final optical density		Kinetics	
Group	CT200 HT901	CY207 HT903	CY207 HT901	CY207 HT903
Associated carboxylic acid				
3000 cm^{-1}	0.045	0.025	Peaks	Peaks
2550 cm^{-1}	0.016	0.009		
Total ester 1725 cm^{-1}	0.36	0.35	1st-order	1st-order
Branched ether				
1140 cm^{-1}	0.115	0.3		
1120 cm^{-1}	0.12	0.3	½-order	½-order
1068 cm^{-1}	0.11	0.23		
Carboxylic acid 1705 cm^{-1} (undeconvoluted)	Too weak	0.125	—	Peaks
Carboxylic acid δ_{-OH}	0.015	0.11	—	—
Total anhydride	—	—	1st-order	1st-order

Postcure Period

During postcure, the reaction continues to completion without limitation, as illustrated by the behavior summarized in Figure 10. During the initial phase of postcure, the hydroxyl group content falls, indicating rapid carboxylic group formation. Its subsequent minimum and rise reflect the competition of monoester consumption and esterification regeneration of hydroxyl groups. In the absence of etherification reaction intermediates, this reaction will conserve the hydroxyl group number. However, rapid hydroxyl group consumption is paralled by the total carboxylic acid (1705 cm^{-1}) behavior, whereas the associated carboxylic group fractions display an induction period. In this respect, the THPA component appears to react initially more rapidly than the PA component, the latter of which displays an induction period also. This suggests that associated carboxylic acid groups are associated with PA reaction. It is interesting also in this context that the associated group content returns after peaking to its starting value, leaving a finite carboxylic group content at the end of cure and indicating that the monoester fragments associated with these groups during postcure are converted to diester linkages or polyester.

Ester formation proceeds with first-order kinetics at 4×10^{-5} s^{-1} and total anhydride consumption proceeds with first-order kinetics at 2.9×10^{-5} s^{-1}. The higher rate of the former, apparent in Figure 10, will occur if rapid diester and polyester reactions occur utilizing the carboxylic acid reservoir established during gelation. In this respect, longer gelation generates a greater carboxylic acid reservoir producing a larger total aromatic ester content. However, the extent of the difference arises from the anhydride behavior during gelation, as seen from comparing the 1732 cm^{-1} optical density in Table I and the THPA and PA behavior in Figure 9. After short (18 h) and long (48 h) gelation, the postcure increase in the $\nu_{C=O}$ optical density is 0.2 and 0.22, respectively. The common

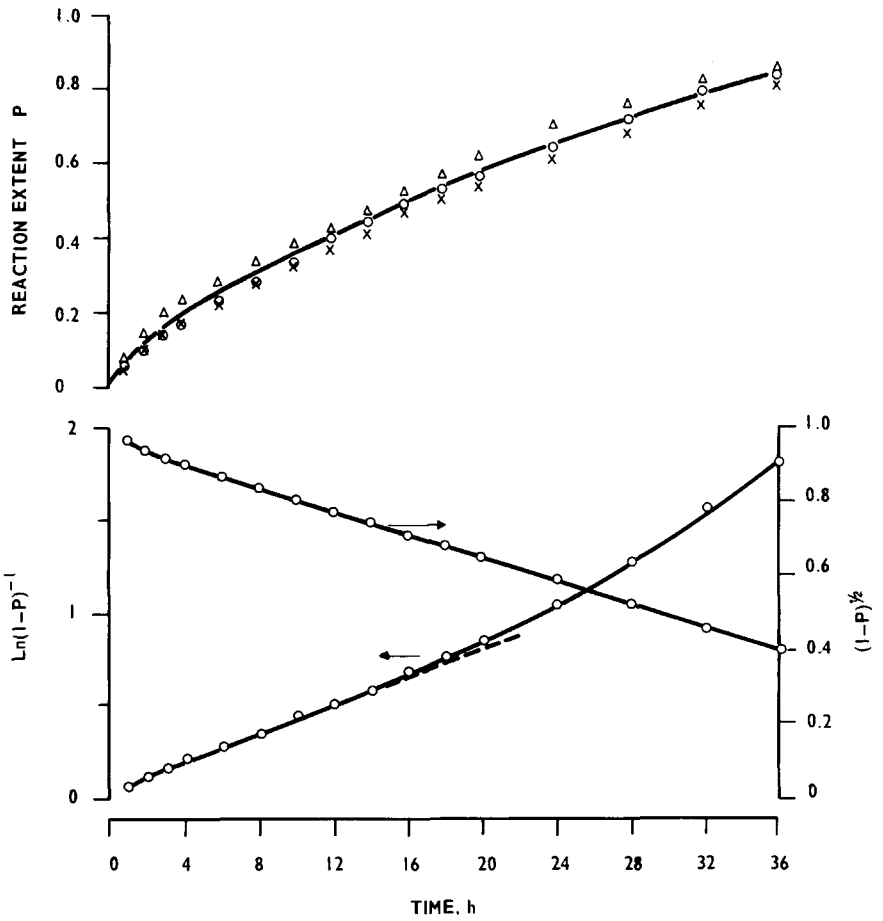

Fig. 8. Branched ether postcure reaction extent and first- and half-order kinetic plots: (△) 1160 cm^{-1}; (○) 1140 cm^{-1}; (×) 1120 cm^{-1}.

feature is that similar quantities of PA have reacted in both cases during gelation. This may be explained if PA reaction during postcure favors diester or polyester formation producing two resultant ester groups per anhydride molecule in comparison with one in THPA. This result would lend support to the associated carboxylic acid species deriving from PA monoester reactions principally and leading to the —COOH 3000 cm^{-1} behavior in Figure 10.

The etherification reaction during postcure proceeds considerably slower than the others and initially is about three times slower than anhydride consumption. The addition etherification reaction of the Fisch and Hofmann scheme requires epoxide groups to be continually available for reaction to proceed. This apparently contradicts the epoxide result, which is 97% complete at 20 h postcure, whereas the ether reaction extent is only 58% complete. This apparent contradiction also occurs in gelation, where the ether step follows the epoxide step. This may be explained by a small number of epoxide groups producing the ether linkages. Alternatively, this may occur as the result of the formation of reaction intermediates which deplete the epoxide content and transform or react further

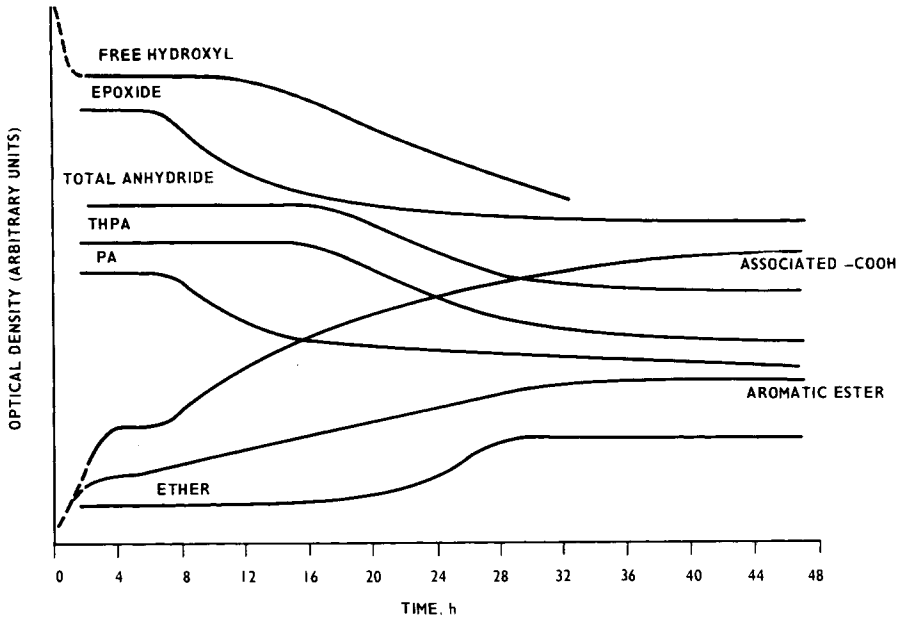

Fig. 9. Chemical group optical density behavior summary of gelatin at 80°C.

at a slower rate to complete etherification. This may also occur in the esterification completion reaction, as suggested by the extended decrease in the associated carboxylic group behavior. Light scattering and DSC glass transition studies to be reported support the extended-period ester and ether reactions. However, no evidence of reaction intermediates was found.

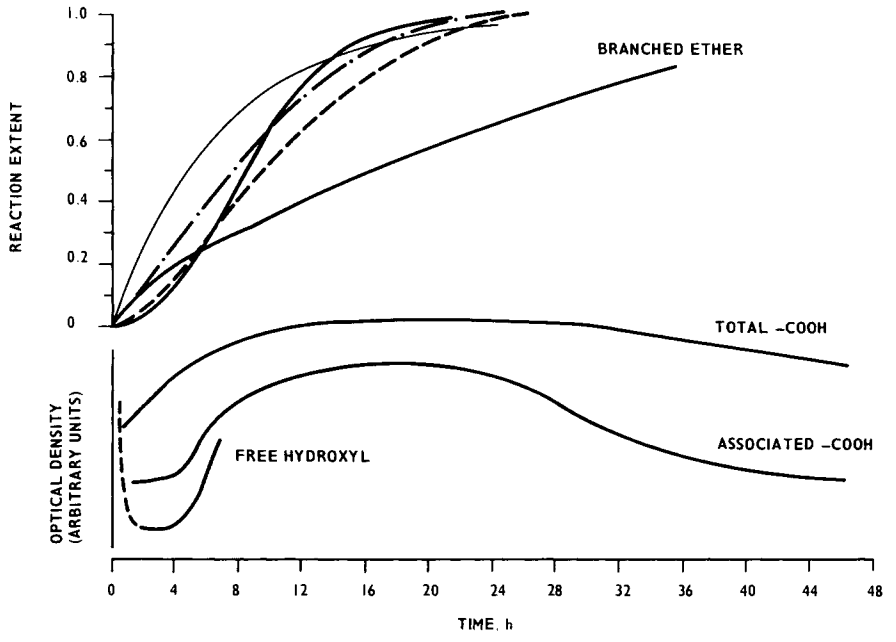

Fig. 10. Chemical group reaction extent and optical density behavior summary of postcure at 120°C after 120°C after 18 h gelation at 80°C: (—) aromatic ester; (-·-) THPA; (- - -) PA; (—) epoxide.

Comparison with CT200–HT901

Table II compares the general kinetic behavior and chemical structure of CT200–HT901 and CY207–HT903 during postcure via optical densities. The ester and branched ether formation kinetics are used to compare formation behavior and not to interpret reaction mechanism directly.

In both systems, addition of the resin and hardener involve rapid hydroxyl–anhydride reactions with formation of a carboxylic acid reservoir. In the CY207, this reservoir is further developed during gelation to promote rapid esterification reactions and aid etherification during postcure. This system also exhibits gelation induction behavior controlled possibly by a matrix effect and the availability of free hydroxyl groups. Anhydride consumption in both systems follows first-order kinetics consistent with hydroxyl group limitation or colloidal-type reactions. The former occurs inherently in CY207. However, light scattering results, to be reported, indicate the presence of molecular aggregates in both resin systems prior to reaction and dramatic optical parameter changes during initial rapid anhydride–hydroxyl reactions which support an hydroxyl group-limited colloidal reaction mechanism.

Aggregate bonding is considered to arise from epoxide–hydroxyl hydrogen bonding and dispersion forces between bisphenol A epoxy resin $k > 0$ molecules. In CY207, a large $k = 0$ oligomer fraction exists acting as a solvent for the $k > 0$ aggregate solute producing smaller aggregates than in CT200, a result confirmed by light scattering. Intermediate anhydride–hydroxyl group reactions will occur preferentially at aggregate surfaces, and the larger proportion of free hydroxyl groups consumed in CY207 (14%) compared with CT200 (8%) indicates a larger aggregate hydroxyl group volume to surface concentration in CT200, consistent with smaller aggregates in CY207.

Subsequent reaction behavior is dependent on aggregate structure, the aggregate–solvent interface, phase stability, and the detailed reaction mechanism of different groups. Aggregate structure and growth will be discussed in further reports. The question of phase stability was raised in connection with the chemical equilibrium regions occurring in CY207–HT903 during gelation. This could occur as a result of gel–sol separation during a homogeneous reaction producing a heterogeneous matrix and an unreactive gel surface. Similarly, an existing heterogeneous matrix involving aggregate nuclei could progress to a similar chemical impasse at the interface. In our case, no evidence exists for a gel–sol phase separation, and the aggregate model is more tenable.

In the low E/H ratio system, the overall reaction proceeds rapidly and supports the step addition reaction scheme of Fisch and Hofmann. In the high E/H ratio system, the slower reaction rates pinpoint the significance of matrix effects and suggest monoester step addition and intermediate structure reactions. In both systems, the importance of free hydroxyl group content in controlling aggregate nature, surface reactivity, and subsequent reaction is clear.

Other comparisons are useful. Both systems display similar ester and branched ether formation kinetics, and with a CY207–HT903 18-h gelation period, the ester contents of both systems are similar. The lower initial total anhydride content in the CT200 system suggests a higher polyester content in this case. The ether content is higher in the CY207 case, consistent with the higher carboxylic acid and epoxide content in this system. Evidence was presented in the CY207–HT903 system suggesting that hydrogen-bonded dimerlike car-

boxylic acid groups derived principally from the phthalic anhydride component. In CT200–HT901, the PA initial content is 23%, whereas in CY207–HT903, it is 15%. Table II indicates a higher associated carboxylic acid fraction in the former system, whereas CY207–HT903 displays a total carboxylic acid content several time greater than in CT200–HT901. This supports the phthalic anhydride connection.

A useful physical property—chemical structure comparison—is provided by the extent of reaction at the gelation point. In our case, the gel point may be defined when an infrared capillary film specimen can no longer be obtained at 80°C. This occurred after 3.5 h in CT200–HT901 and 7.5 h in the postcure of CY207–HT903 after an 18-h gelation period. Table III summarizes the reaction extent and group concentration ratios of both systems at their gel points. Distinction between homogeneous and heterogeneous reaction mechanisms may be attempted by considering the reaction extent required for chemical gelation of a homogeneous system and the criterion required for heterogeneous gelation. The latter has not been considered formally. Critical chemical conditions for the formation of infinite networks (gelation) in homogeneous systems has been discussed by Flory[5] in terms of the functionality of the system and a statistical approach to assess the probability of extended chain branching. It suffices to indicate that the anhydride reaction extent required for gelation in a high-functionality system such as CT200 should be lower than in a lower-functionality system such as CY207. The converse is true in the results of Table III.

The similarity in the reaction behavior of low and high epoxide/hydroxyl group ratio bisphenol A epoxy resin–anhydride systems is considered to arise from an hydroxyl group-limited inhomogeneous reaction mechanism involving molecular aggregates present in the resins prior to reaction. In this, free hydroxyl group content is important in aggregate formation, in aggregate surface chemistry, and in controlling reaction progression. Thus, the final matrix sturcture will be aggregate dependent as well as functional-group, reactant-stoichiometry, and reaction-condition dependent. These latter points provide their own final structure prediction as summarized by Lee and Nevill,[6] and the chemical structure comparisons of Table II are generally in agreement with these. However, the detailed behavior is not.

Interesting parallels exist with the polyesterification reactions of alkyd resins in which reaction homogeneity and the constancy of hydroxyl group reactivity was called into question. The works of Solomon and Hopwood,[7] Solomon, Loft, and Swift,[8] and Solomon[9] invoke the formation of microgel particles and an heterogeneous reacting volume for systems with functionality greater than 2. In the early stages of polymerization, some molecules exhibit potential surface activity. These form micelles at whose surface rapid polyesterification occurs

TABLE III

Group	Reaction extent,% CT200	CY207	C_{CY207}/C_{CT200}
Total anhydride	64	52	0.81
Aromatic ester	54	81	1.44
Branched ether	48	47	2.43

with the eventual formation of microgel particles. These particles exhibit reduced activity since they are no longer in the same phase as the other reacting moieties and phase separation or phase inversion may occur.

CONCLUSIONS

The high epoxide/hydroxyl group-ratio bisphenol A epoxy resin–anhydride system chemically reacts by consecutive-step addition esterification involving carboxylic acid group intermediates and simultaneous addition etherification in agreement with the reaction scheme of Fisch and Hofmann. Hydrogen-bonded carboxylic acid groups occur and derive principally from the phthalic anhydride reaction, whereas during postcure, monoester fragments derive principally from the tetrahydrophthalic anhydride reaction.

The gelation reaction is complex, initially involving rapid resin hydroxyl–anhydride reactions establishing a carboxylic acid reservoir containing a proportion of hydrogen-bonded pairs. This is followed by an induction period involving little or no reaction and an S-shaped reaction behavior, for all groups, to an incompletely reacted limit which does not lead to physical gelation. Postcure completes the reaction. Total anhydride consumption follows first-order kinetics with a rate constant of $2.9 \times 10^{-5}\ s^{-1}$, and ester formation proceeds with first-order kinetics and a rate constant of $4 \times 10^{-5}\ s^{-1}$, utilizing the gelation-generated carboxylic acid reservoir. Phthalic anhydride and tetrahydrophthalic anhydride compete for hydroxyl groups, and both display half-order kinetics with differing reactivities. Epoxide consumption exibits S-shaped kinetics, and branched ether formation displays half-order kinetics, considerably slower than all other reactions.

The reaction behavior of low and high epoxide/hydroxyl-group ratio bisphenol A epoxy resin–anhydride systems are similar. This is considered to arise from an hydroxyl-limited inhomogeneous reaction mechanism involving molecular aggreates present in the DGEBA resins prior to reaction. In this model, free hydroxyl-group content is important in controlling aggregate formation and size, aggregate surface chemistry, and reaction progression.

The author wishes to thank Mrs. Marion Redfearn for her general assistance. This work was undertaken at the General Electricity Research Laboratories and is published by permission of the Central Electricity Generating Board.

References

1. W. Fisch and W. Hofmann, *J. Polym. Sci.*, **XII,** 497 (1954).
2. G. C. Stevens, J. V. Champion, P. Liddell, and A. Dandridge, *Chem. Phys. Letts.*, **71**(1), 104 (1980).
3. G. C. Stevens, J. V. Champion, and P. Liddell, *J. Polym. Sci. Polym. Phys.*, to appear.
4. G. C. Stevens, J. V. Champion, and P. Liddell, to appear.
5. P. J. Flory, *Principles of Polymer Chemistry*, Cornell University Press, New York, 1978.
6. H. Lee and K. Neville, *Handbook of Epoxy Resins*, McGraw-Hill, New York, 1967.
7. D. H. Solomon and J. J. Hopwood, *J. Appl. Polym. Sci.*, **10,** 981 (1966); *ibid.*, **10,** 1893 (1966).
8. D. H. Solomon, B. C. Loft, and J. D. Swift, *J. Appl. Polym. Sci.*, **11,** 1593, (1967).

9. D. H. Solomon, *J. Macromol. Sci. Revs.*, C1(1), 179 (1967); *ibid.*, in *Step-Growth Polymerizations*, Marcel Dekker, New York, 1972, Chap. 1.

Received April 21, 1980
Accepted April 28, 1981